Experimental and numerical study of radial flow and its contribution to wake development of a HAWT

Daniel Micallef[1,2], Buşra Akay[1], Tonio Sant[2], Carlos Simão Ferreira[1], Gerard van Bussel[1]

[1]DUWIND, TUDelft, Faculty of Aerospace Engineering, Kluyverweg 1, 2629 HS, Delft, The Netherlands
[2]University of Malta, Faculty of Engineering, Department of Mechanical Eng., Msida, MSD 2080 Malta.

Keywords: Horizontal axis wind-turbine, radial flow, wake expansion

Abstract:

The scope of this work was to investigate radial flow component for a Horizontal Axis Wind Turbine in axial flow conditions and to assess its impact on the turbine operation. This was done by means of Particle Image Velocimetry and numerical simulation with a 3D unsteady potential-flow panel model. A direct comparison between the numerical and experimental radial velocity results show differences in the tip and root regions. These differences have important implications on the wake development just at the moment of release of the tip vortex. Moreover, the impact of the radial velocities on the blade loading has been studied using the numerical results. The contribution of the radial velocity to the normal load on the blade is only slightly appreciable in the tip and root regions of the blade. However, as the numerical model does not account for viscous effects, further analysis of impact on boundary layer development is necessary.

Nomenclature

r = radial position [m]
R = Rotor radius [m]
θ = Twist [deg.]
μ = Doublet strength [m^3/s]
∇ = Differential operator
Φ = Velocity potential [m^2/s]
S = Surface of integration [m^2]
σ = Source strength [m^3/s]
x = distance from a particular point in the flow field [m]
$\partial/\partial n$ = differential operator along the normal direction [m^{-1}]
ϵ = error estimator
p = order of the numerical method used in the simulation
η = the ratio of the number of panels used for the simulation against a reference simulation
R_{hub} = Rotor hub radius [m]
D = Rotor diameter [m]
C_p = Pressure coefficient
V = Absolute velocity [m/s]
V_{ref} = Reference velocity [m/s]
t = Time [s]
ρ = Air density [kg/m^3]
F = Force per unit length [N/m]

Subscripts:
u = Upper surface of the airfoil (suction side)
l = Lower surface of the airfoil (pressure side)
w = Wake
B = Body
∞ = Free-stream
ref = Reference simulation (one having a fine discretization and a high number of revolutions)

Abbreviations:
OJF - Open Jet Facility
SPIV - Stereo Particle Image Velocimetry
NREL - National Renewable Energy Laboratory
UAE - Unsteady aerodynamics experiment
MEXICO - Model experiment in controlled conditions
FOV - Field of view
GCI - Grid convergence index

1 Introduction and Research Questions

The radial component of the flow perceived by the rotor blade is a result of the apparent flow motion in the rotating reference frame and the radial induction of the flow in the inertial reference frame. In this research paper, we experimentally and numerically analyze the latter. A 2m diameter, two-bladed wind-turbine model was tested in the Open Jet Facility (OJF) at Delft University of Technology. Stereo Particle Image Velocimetry (SPIV) was used to determine the velocity field over the blades as well as in the wake. The experiment was simulated using a potential-flow panel method to investigate the radial flow and its contribution to the wake's development.

The numerical simulations were validated with the experimental data and used to analyze the source of the radial expansion.

Flow velocities were measured in past experiments using PIV as well as hot-wire anemometry. An overview of wind-turbine wake research at TUDelft is given by Vermeer [1].For a wind-turbine in axial flow, the radial component of velocity is due to the wake induction and the bound circulation and blockage of the blade. Much of the focus in literature is placed on the effect that radial velocity has on the stability of the boundary layer in the root region of the blade resulting in stall delay. The NREL Unsteady Aerodynamics Experiment (UAE) [2] and the Model Experiment in Controlled Conditions (MEXICO) [3] revealed the dramatic effects that radial flows have in the root region. Schreck et al. give an excellent review (especially of the findings from the NREL UAE phase VI experiments) in [4]. Moreover, some recent results have also been obtained for the MEXICO experiment by Schepers et al. [5] and Schreck et al. [6]. Various experimental studies have been conducted which report radial velocities in the wake such as by Medici et al.[7] at locations 1D downstream. At these distances from the rotor plane, radial components are almost negligible. Ebert et al. [8, 9, 10] show the velocity components at around 1.5 chord lengths downstream. The tip vortex was found to have a relatively high impact in the tip region. A lifting-line numerical model was used by Sant et al. [11, 12] and radial velocities on the blade lifting line were established for the NREL phase VI rotor. Sant found that radial components (due to the wake) are directed outwards at the tip region and inwards towards the hub in the root region for the case of attached flow. This was not found for the separated flow cases. The causes of this behaviour are not discussed in detail and the effects of the nacelle were not included. In this work we address radial velocities in the outer flow (external to the boundary layer) since, as was shown in the referred literature, it has fundamental implications on the sectional airfoil behaviour. The aims of this study are therefore as follows:

1. Shed light on the impact that radial velocity has on the wake development by means of computational results

2. Build upon the current knowledge on the three-dimensionality of wind-turbine flow

3. Investigate the relevance of radial flows for wind-turbine blade design in particular how the radial flow impacts the loading

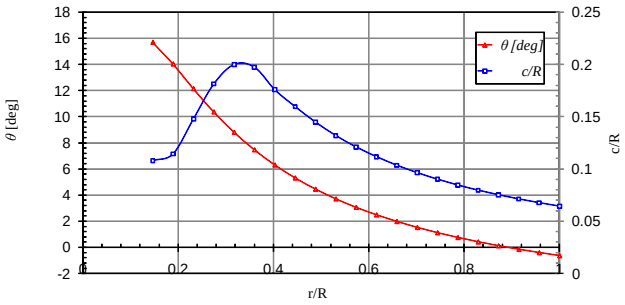

Figure 1: Twist and chord distribution along the blade.

Yaw angle	0
Wind speed	6 m/s
Pitch	0
Tip speed ratio	7
Thrust coefficient	0.87
Power coefficient	0.44

Table 1: Experimental wind-turbine specifications

2 Experimental Setup

In the SPIV experiment, the model wind-turbine model was tested in the OJF wind tunnel at TUDelft, which has an octagonal jet with equivalent diameter of 3 m. Figure 1 shows the chord and twist distributions of the blade. The airfoil section used was a DU96-W180 throughout the entire span of the blade except at the connection point with the hub (nacelle). The tip radius was 1 m while the hub radius was 0.147 m. The rotor had two blades and rotated in a clock-wise direction when looking downwind. The test conditions used in this experiment are summarised in table 1.

Spanwise measurements were performed to quantify the flow field.The laser sheet was on a horizontal plane with the cameras viewing from below. For this setup, a Field of View (FOV) of around 265mm x 194mm was used. The angles between the cameras was set to approximately 40°. Measurements were taken at five spanwise locations (covering the entire blade span) and for each location, images were taken for various azimuthal positions. This ensured that the flow field was captured for the entire blade passage through the horizontal plane. In order to account for shadowing effects, images were taken from an upwind and downwind directions. A single field-of-view result was composed of the several measurements at different spanwise and azimuthal positions; these results are presented in this paper. Figure 2 shows the camera-laser con-

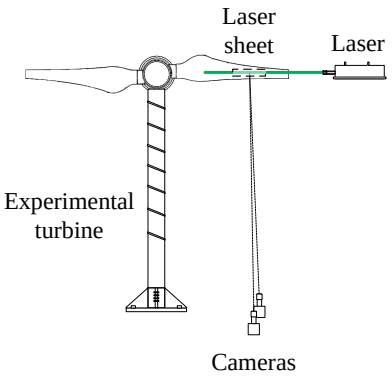

Figure 2: Measurements in the spanwise direction.

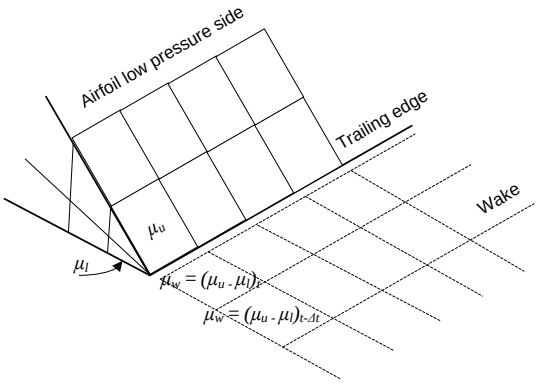

Figure 3: Panel representation of the wing and the release of panels representing the wake.

figuration used to perform the measurements.

3 Potential Flow Solver

The experimental turbine was modelled using a 3D unsteady potential-flow panel-method with a free-wake model as described in the work of Dixon [13]. To model a 3D body, the surface is approximated by a number of doublet and source panels. As the blades rotate, a wake of free-convecting doublets is released from the trailing edge. The panel model uses a Dirichlet boundary condition. This can then be used to evaluate the velocities by means of differentiating the potential function given by [14]:

$$\nabla\Phi = -\frac{1}{4\pi}\int_{S_B}\sigma\nabla\left(\frac{1}{x}\right)ds + \frac{1}{4\pi}\int_{S_B+S_W}\mu\nabla\left[\frac{\partial}{\partial n}\left(\frac{1}{x}\right)\right]dS + \nabla\Phi_\infty \quad (1)$$

Figure 3 represents the body having doublet strengths μ_u and μ_l on the suction and pressure side of the airfoil respectively. Source terms on the upper and lower surfaces should also be included but are not shown in the figure to keep it uncluttered. According to the Kutta condition, the vorticity at the trailing edge should be zero. Thus, the wake doublet strength is given by the difference in doublet strengths of the upper and lower surfaces of the body. The model may be used to simulate the behaviours of multiple bodies such as for instance the blades, nacelle and tower. The formulation used in this model is an unsteady approach and therefore can account for unsteady effects. More detail can be found in [14]. Thorough validation of the model was carried out by Dixon [13] and Ferreira [15].

The simulated body includes both blades, hub and nacelle. Solution convergence was checked by studying the convergence of bound circulation as well as velocities at various points in the flow field. The method proposed in [16] was used to obtain an estimate of the Grid Convergence index (GCI) which is defined as follows:

$$GCI = \frac{|\epsilon|\,\eta^p}{\eta^p - 1} \quad (2)$$

Where p is the order of the numerical method used (here taken as 1), η is the ratio of the total number of panels used to the total number of panels used in a reference simulation (having a fine discretization and a large number of rotor revolutions) and ϵ is an error estimator given by:

$$\epsilon = \frac{f - f_{ref}}{f_{ref}} \quad (3)$$

Where f is the value of a particular variable from the solution and f_{ref} is the same value but for the reference simulation.

Two types of checks were carried out:

1. Independence of blade and wake discretisation by having a coarse, moderate and fine discretisation of the blades (and hence of the shed wake): The GCI of the bound circulation and velocities at various points converged to within 4% with a fine mesh setting.

2. Independence from the number of rotor revolutions: The convergence errors are shown in figure 4. All quantities fall below 3% after 13 wake revolutions.

The input parameters for the fine mesh simulation are summarised in table 2. The operating conditions of wind speed and rotor speed of the experiment were used as input.

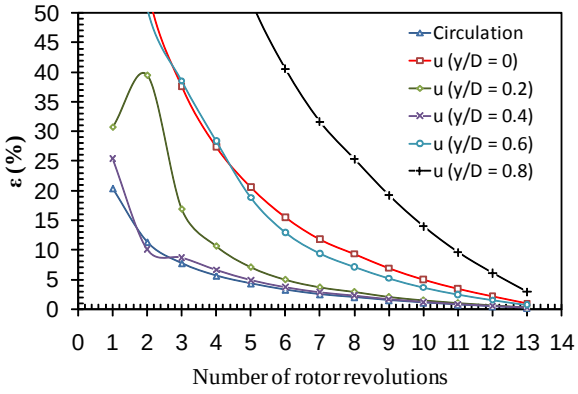

Figure 4: Convergence of bound circulation and axial velocities for increasing number of revolutions. Velocity convergence is shown at 5 different downstream positions (at x/D = 0.25).

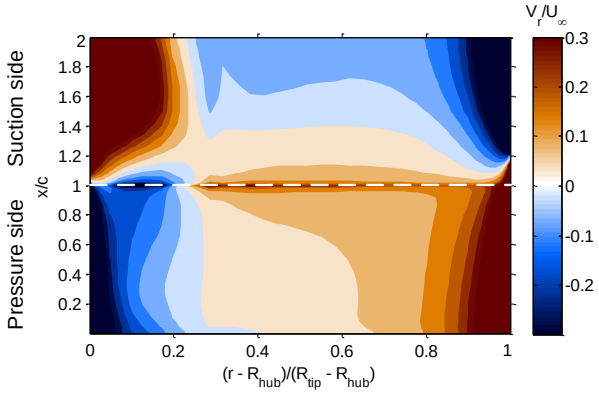

Figure 5: Contour plot of normalised radial velocities on the blade surface. The parameter x/c represents normalized chordwise position traversing from the trailing edge (0) to the leading edge (1) of the pressure side and proceeding to the suction side (1 to 2).

Blade spanwise panels	46
Blade chordwise panels	38
Nacelle spanwise panels	50
Nacelle circumferential panels	50
Azimuthal step	10°
No. of rotor revolutions	14
Vortex model	Ramasamy-Leishman [17, 18]
Core growth model	Ramasamy-Leishman [17, 18]

Table 2: - Input parameters for the panel code simulation.

4 Results

Due to the inviscid assumption of the flow in the model which was used, the velocities only represent velocities which are outside of the blade boundary layer. The experimental results would help in clarifying the effects of viscosity especially in the sensitive regions such as the tip. However, the velocities obtained from PIV, very close to the blade surface tend to be inaccurate due to reflections on the blade surface. A direct comparison of the radial velocities on the blade surface with the potential flow model cannot be made. Hence, only the absolute radial velocities obtained from the potential-flow model are shown in figure 5. Positive radial velocity is directed from root to tip. The edge effects are immediately apparent with opposite directions on the suction and pressure side and with magnitudes that reach and exceed the free stream velocity. The root radial velocity, which is the source of stall delay, influences up to around 25% of the blade span (on the suction side). In this region, on the suction side, a curve of practically zero radial velocity can be observed which stretches from the trailing edge at around 20% span to the leading edge just at the blade root. More outboard to this line, in the mid-board region, these radial flow components are relatively small. The radial velocities due to the tip vortex on the suction side influence up to around 85% of the blade span. The radial momentum change, as the wake is released from the blade, must be equal to the radial loads present on the blade. These radial loads have also been hypothesized by van Kuik [19] due to an inconsistency in the actuator disc momentum theory.

Figures 6, 7 and 8 show a cross section of the wake through the 90 degree position (0 degrees is the position of the upright blade), when the blade is located at 80, 90 and 100 degrees. The blade passage can be observed at the 90 degree azimuth position. For each of these figures, the top left diagrams show the corresponding blade azimuthal position, the top right contour plots show the calculated radial velocities on a horizontal plane while the middle figures shows the detailed radial velocities calculated at the rotor plane. Finally the bottom figures shows the experimental radial velocity contours. Induced velocity vectors are also superimposed on all contour plots. The calculated velocities enable a much broader view of the flow field compared to the SPIV results which only show the rotor plane regions. Along the interior of the wake (the region between the root and tip vortices), the radial velocity components are relatively low but most of the flow field is governed by an outward radial component. The root and tip vortices are clearly visible by a positive and negative radial velocity. The net velocity on the tip vortex clearly appears to be pointing outwards

to cause the well known wake expansion. Towards the root region, root vortex-nacelle interaction takes place. Simulations without the nacelle have shown that the root vortices also have a net radial inward velocity. This was also pointed out by Sant in [11] for the NREL rotor. However, due to the interaction with the nacelle no such inboard motion of the root vortices can be observed. When the blade quarter chord line just traverses the 90 degree plane the radial velocities at the edge of the streamtube increase quite substantially. This supports the observations made from figure 5 that the blade influence in the flow three-dimensionality is substantial towards the root and tip regions. Due to the large chord towards the root region of the blade, the presence of the blade can still be seen at 100 degrees. The magnitudes of the radial components found in this study are comparable to the experiments by Medici et al. [7] and Ebert et al.[10].

The experimentally observed velocities at the rotor plane show the same trends as obtained numerically. At the 80°blade position, an inboard radial velocity region may be observed towards the root region and an outboard radial velocity in the tip region. The magnitudes of the velocities however seem to be lower those found numerically. It was also clear that the axial velocity vectors are much larger close to the blade mid-span than those found experimentally. The sources of these differences is still unclear but could be due to numerical integration issues or even the use of empirical inputs in the potential flow model such as the initial core radius. At the 90°position, the experimental result shows a much lower radial velocity component compared to the panel model simulation. Still, a predominantly outboard radial velocity trend may be observed in the root region. Towards the tip, the tip vortex seems to effect up to the 80% span position of the blade. This effect was not captured by the simulation. In this case, the axial induction vectors midboard seem to be much larger than those found numerically. These differences could mean that there are difference in the peak circulation in this blade region. At the 100°position, no experimental data is available close to the tip of the blade and hence, the effect of the tip vortex can only just be observed. It must be said, that for this blade position, the blade may appear thicker. This is actually the shadowing effect of the blade. At x/D = 0.1 a small region of inboard radial flow can be observed exclusively from the experimental results. The effect of the root vortex was again much less pronounced than that found from the simulations. At this blade position, as also suggested by the simulations, the radial velocity on the downstream location of the rotor plane, the radial velocity is predominantly outboard. These experimental observations underline the strong tendency for the wake to expand just behind the rotor plane. If we consider the tip region for instance, all of the downwind tip-vortices, especially the newly released tip vortex, cause a high radial expansion close to the rotor plane. As seen from the simulations, the radial velocities downwind decrease due to the dissipation of the tip vortices.

Although the radial components of velocities on and the blade and close to the blade surface were found to be quite large, the question still remains whether the loads generated by these flow components could be of relevance to wind-turbine designers. The radial aerodynamic loads may in fact be negligible compared to the mechanical stress generated by centrifugal forces due to rotation. No load information was gathered in the SPIV experiment. From the panel code simulations it was however possible to obtain the loads acting on the blade from the of pressures on the blade surface. For the unsteady potential flow model, the pressure coefficient on each panel was found from:

$$C_p = 1 - \left(\frac{V}{V_{ref}}\right)^2 - \frac{2}{V_{ref}^2}\frac{\partial \Phi}{\partial t} \qquad (4)$$

where V_{ref} is the reference velocity (taken as the wind speed) and V is the absolute velocity on each panel. A comparison between the blade normal, tangential and spanwise force coefficients is shown in figure 9. It is apparent that the normal force coefficient is the predominant quantity and that the radial force is the smallest component. However it is interesting to also check the effect of the radial velocity on the normal force coefficient. Figure 10 shows a comparison between the normal force coefficient with and without the inclusion of the radial velocity in the calculation of the pressure coefficient. The importance of the results from figure 5 are highlighted here. In regions of high radial velocity (root and tip) the normal force coefficient changes appreciably when the radial velocity components are eliminated. This effect is particularly prevalent in the root region.

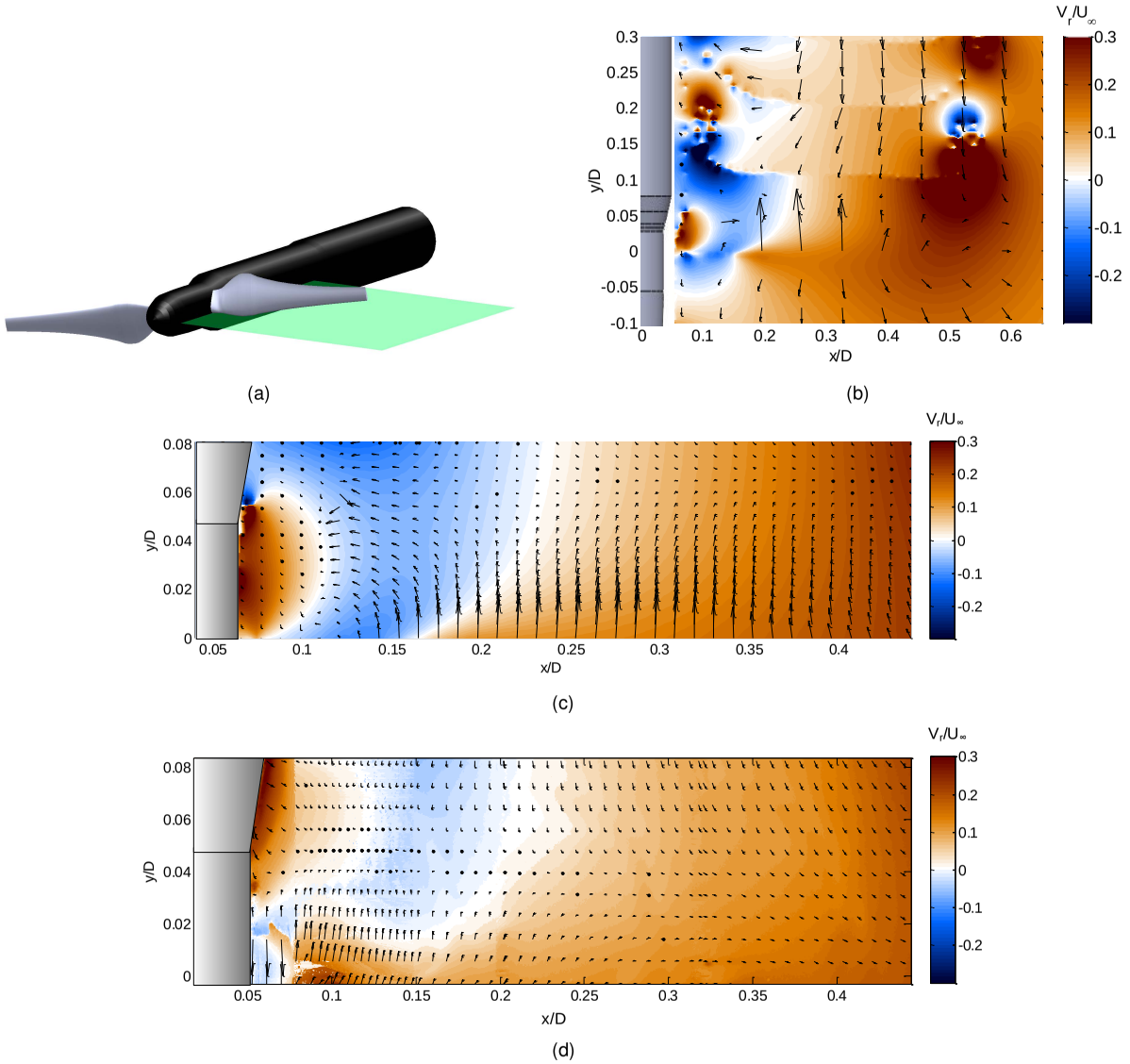

Figure 6: Blade position at 80 degrees. Top-left figure shows blade position, top right figure shows computed radial velocities on a horizontal plane as obtained from the panel model, central figure shows computed velocities at the rotor plane only and bottom figure shows velocities in the rotor plane as obtained from the experiment.

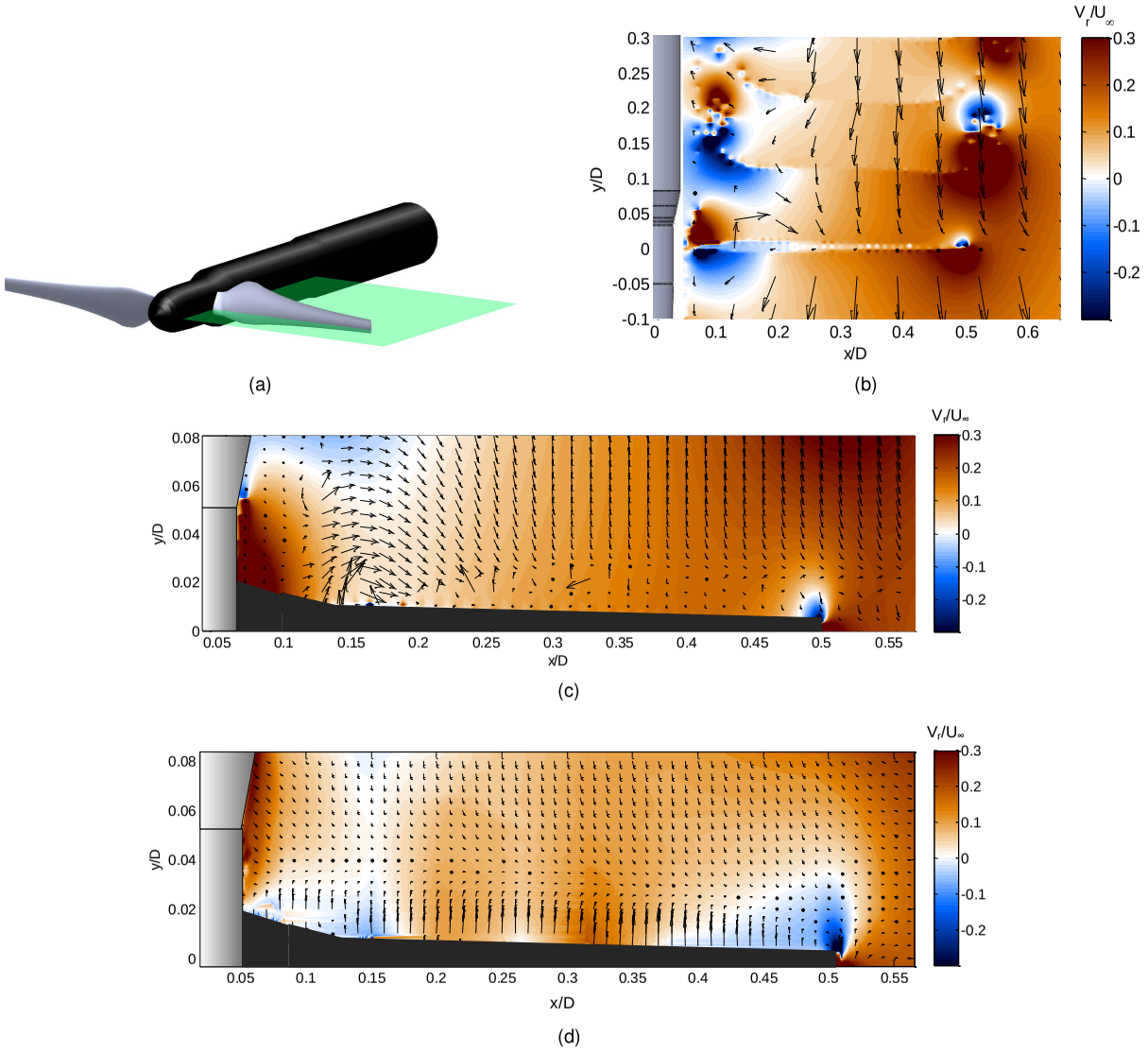

Figure 7: Blade position at 90 degrees. Top-left figure shows blade position, top right figure shows computed radial velocities on a horizontal plane as obtained from the panel model, central figure shows computed velocities at the rotor plane only and bottom figure shows velocities in the rotor plane as obtained from the experiment.

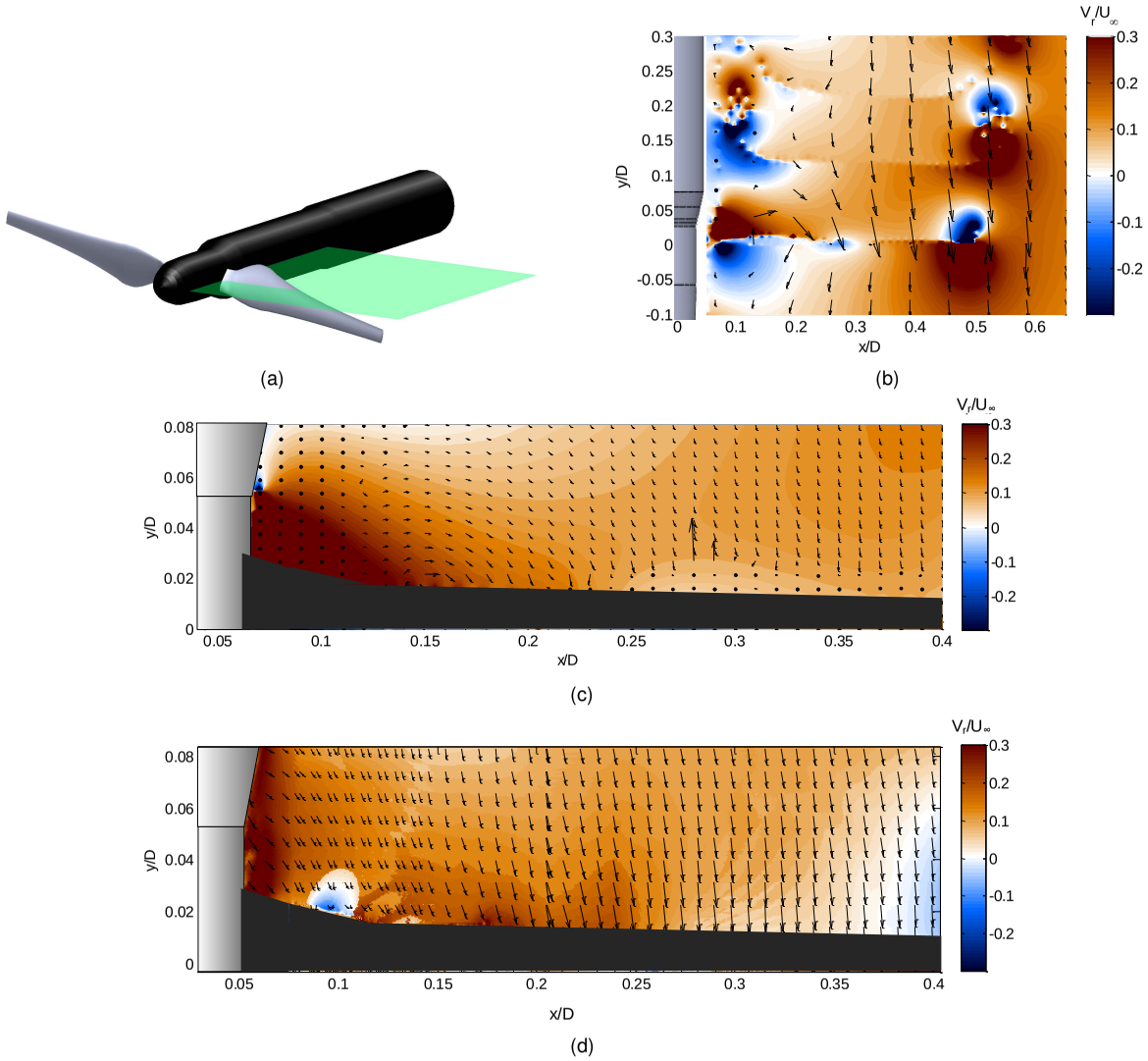

Figure 8: Blade position at 100 degrees. Top-left figure shows blade position, top right figure shows computed radial velocities on a horizontal plane as obtained from the panel model, central figure shows computed velocities at the rotor plane only and bottom figure shows velocities in the rotor plane as obtained from the experiment.

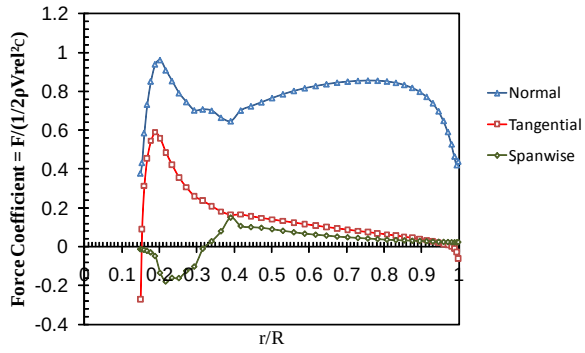

Figure 9: Force coefficient against non-dimensionalised radius as obtained from the potential flow simulations (effects of friction drag cannot be included). Normal, tangential and spanwise coefficients are shown.

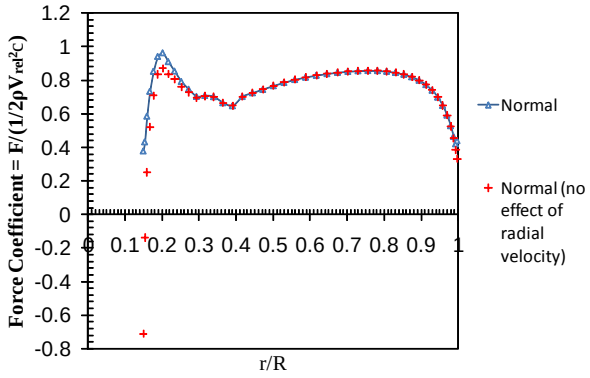

Figure 10: Normal force coefficient against non-dimensionalised radius compared to the same quantity but without the effect of the radial velocity in the calculation of the blade forces.

5 Conclusion

This work explores the behaviour of the radial flow velocity, for an axial flow wind-turbine. To this end, SPIV experimental results have been used. To better understand the flow physics, a panel model has been adopted. The evolution and expansion of the wake could hence be explained from the complex interaction of the tip vortices. The description of the radial flow velocity on the blade leads to better understanding of the relevance of blade radial loads which were investigated for the actuator disc case by van Kuik et al. [19].

In conclusion it may be stated that radial flows predominate in the root and tip regions of the blade with directions corresponding to the orientations of the root and tip vortices. In the mid-board region the radial components are relatively small. Nacelle-root vortex interaction was observed experimentally as well as numerically. Moreover, the radial loads for axial flow conditions are small especially when compared to the normal force component. It was also shown that if the radial velocity contribution to the pressure distribution was ignored, only a slight effect on the normal force coefficient results in the root and tip regions. Nonetheless, it must be emphasized that a viscous analysis is required to completely understand the effects on the loading. In future work, chordwise measurements will be considered. Also, for yawed flow, it can be hypothesized that radial flows play a much more important part. This will also be studied in later work.

References

[1] L. Vermeer, “A review of wind turbine wake research at TUdelft,” in *A Collection of the 2001 ASME Wind Energy Symposium Technical Papers*, pp. pp 103–113, 21-23 May 2001.

[2] M. Hand, D. Simms, L. Fingersh, D. Jager, J. Cotrell, S. Schreck, and S. Larwood, “Unsteady Aerodynamics Experiment Phase VI: Wind Tunnel Test Configurations and Available Data Campaigns.” Technical Report NREL/TP-500-29955, National Renewable Energy Laboratory 1617 Cole Boulevard Golden, Colorado 80401-3393, 2001.

[3] J. G. Schepers and H. Snel, “Model experiments in controlled conditions(MEXICO),” June 2007. ECN-E-07-042.

[4] S. J. Schreck and M. C. Robinson, “Horizontal axis wind turbine blade aerodynamics in experiments and modeling,” *Energy Conversion, IEEE Transactions on*, vol. 22, pp. 61 –70, mar. 2007.

[5] G. Schepers, K. Boorsma, and H. Snel, “Iea task 29 mexnext: Analysis of wind tunnel measurements from the eu project mexico,” in *3rd Torque 2010 The Science of making Torque from Wind Conference*, (FORTH, Heraklion, Crete, Greece), June 28-30 2010.

[6] S. Schreck, T.Sant, and D. Micallef, “Rotational augmentation disparities in the mexico and uae phase vi experiments,” in *3rd Torque 2010 The Science of making Torque from Wind Conference*, (FORTH, Heraklion, Crete, Greece), June 28-30 2010.

[7] D. Medici and P. Andersson, “Measurements on a wind turbine wake 3d effects and bluff

body vortex shedding," *Wind Energy Journal*, vol. 9, pp. 219 – 236, 2006.

[8] P. Ebert and D. Wood, "The near wake of a model horizontal-axis wind turbine - i experimental arrangements and initial results," *Renewable Energy*, vol. 12, pp. 225–243, 1997.

[9] P. Ebert and D. Wood, "The near wake of a model horizontal-axis wind turbine - ii. general features of the three-dimensional flowfield," *Renewable Energy*, vol. 18, pp. 513–534, 1999.

[10] P. Ebert and D. Wood, "The near wake of a model horizontal-axis wind turbine part 3: Properties of the tip and hub vortices," *Renewable Energy*, vol. 22, pp. 461–472, 2001.

[11] T. Sant, G. van Bussel, and G. van Kuik, "Estimating the angle of attack from blade pressure measurements on the nrel phase vi rotor using a free wake vortex model: Axial conditions," *Wind Energy Journal*, vol. 9, pp. 549–577, 2006.

[12] T. Sant, *Improving BEM based aerodynamic models in wind turbine design codes*. PhD thesis, Technische Universiteit Delft, 2007.

[13] K. Dixon, "The near wake structure of a vertical axis wind turbine," Master's thesis, Technische Universiteit Delft, 2008.

[14] J. Katz and A. Plotkin, *Low-Speed Aerodynamics*. Cambridge University Press, second ed., 2001.

[15] C. S. Ferreira, *The Near Wake of the VAWT*. PhD thesis, Technische Universiteit Delft, 2009.

[16] P. J. Roache, *Verification and Validation in Computational Science and Engineering*, pp. 107–141. Hermosa Publishers, 1998.

[17] M. Ramasamy and J. G. Leishman, "A generalized model for transitional blade tip vortices," *Journal of the American Helicopter Society*, vol. 51, no. 1, pp. 92–103, 2006.

[18] M. Ramasamy and J. G. Leishman, "A reynolds number-based blade tip vortex model," *Journal of the American Helicopter Society*, vol. 52, no. 3, pp. 214–223, 2007.

[19] G. van Kuik and A. van Zuylen, "On actuator disc force fields generating wake vorticity," in *Proc. 508 Euromech Colloquium on wind turbine wakes*, (Madrid, Spain), October 2009.

Acknowledgments

The research work disclosed in this publication is partially funded by Malta Government Scholarship Scheme grant number MGSS PHD 2008-11, Vestas and TUDelft. The authors also acknowledge the assistance of B. Geurts during the experiment.